

Electronic Supplementary Material

Deciphering Anisotropic Energy Harvesting Responses of an Above Room Temperature Molecular Ferroelectric Copper(II) Complex Single Crystal

Rajashi Haldar, ^{a, ‡} Ajay Kumar, ^{b, ‡} Dipankar Mandal, ^{b, *} Maheswaran Shanmugam ^{a, *}

[a] Rajashi Haldar, Maheswaran Shanmugam
Department of Chemistry,
Indian Institute of Technology Bombay,
Powai, Mumbai-400076, Maharashtra, India
E-mail: eswar@chem.iitb.ac.in (MS)

[b] Ajay Kumar, Dipankar Mandal
Quantum Materials and Devices Unit,
Institute of Nano Science and Technology Mohali
Knowledge City, Sector 81, Mohali 140306, India
E-mail: dmandal@inst.ac.in (DM)

‡ Authors contributed equally

Experimental section:

Materials and Methods: All of the chemical reagents in the synthesis were of reagent grade and used without further purification.

Single crystal X-ray diffraction measurement: The single-crystal diffraction data of the complex was collected on a Bruker diffractometer with Mo K α radiation ($\lambda = 0.71073 \text{ \AA}$). Data reduction and the unit cell parameters were determined by using CrysAlisPro 1.171.38.43. With the help of Olex2 software with the SHELXL program, crystal data was solved by direct method and refined by the least square procedure. All non-hydrogen atoms were refined anisotropically and the positions of all hydrogen atoms were generated geometrically. The data collection and structure refinement of these crystals are summarized in Table S1. **Powder X-ray diffraction (PXRD):** Powder XRD measurements were carried out in a Rigaku D/tex Ultra 250 instrument, using Cu K β filter with a scan speed of 5° /min at room temperature and at variable temperatures. Diffraction patterns were collected in the 2 θ range of 5–50° with a step size of 0.01°. **Hirshfeld surface analysis:** The Hirshfeld surface mapping of all the non-covalent molecular interactions of complex **1** was done using the Crystal Explorer 3.1 program. The single-crystal X-ray crystallographic information file (CIF) was utilized to visualize all the different type of interactions which are present on the Hirshfeld surface. These interactions were obtained as 3D color mapping images such as normalized contact distance (dnorm), shape index and curvedness. The diverse surface colour mappings were generated on the Hirshfeld surface by various colour coding based on strong (red), medium (blue) and weak (white) interactions. **Thermal analyses:** Differential Scanning Calorimetry was done using a Perkin Elmer Pyris 6 DSC instrument by heating and cooling crystalline samples with a rate of 5 K min⁻¹ in aluminium crucibles at nitrogen atmosphere. Thermogravimetric analyses (TGA) were carried out on a TA TGA-55 instrument by heating crystalline samples with a rate of 10 K/min under nitrogen atmosphere. **Dielectric and ferroelectric measurement:** Complex dielectric permittivity was measured with Keysight Impedance Analyzer E4990A system, where two parallel plate capacitor geometry is considered. Silver conductive paste deposited on both sides of the pressed pellets of the sample were used as top and bottom electrodes. Ferroelectric measurements were also performed on pressed pellets using a Radiant Precision II ferroelectric loop tracer with trek high voltage amplifier of Radiant Technologies USA.

Pyroelectric measurement:

Pyroelectric measurements were performed by in-house customised setup, where Infra-red lamp (150 W, Murphy, India) was used with GW Instek SFG 1013 function generator and chopper circuit (frequency 0.1 Hz) to control the heating and cooling of the crystal. The temporal change in temperature was measured with a thermocouple and the pyroelectric current was recorded by using Keithley SMU 2450.

PFM measurement: Local topography, piezoelectric properties and ferroelectric switching were studied on a pure single crystal of size $0.24 \times 0.37 \times 0.50 \text{ mm}^3$ by scanning probe microscopy (SPM) technique using piezo-response force microscopy (PFM) in DART (Dual AC Resonance Tracking) mode, in a MFP-3D BIO instrument (Asylum Research) using an SCM-PIT-V2 probe. The amplitude and phase images were recorded by applying fixed ac voltage and the typical butterfly loops and phase loops were recorded by applying different DC biases to tip with the ac voltage.

Synthetic procedure for 1:

The material was synthesized following the procedure described by Subramaniam et al. (*Inorg. Chem.* 2001, **40**, 4291–4301). A mixture of L-phenylalanine (0.826 g, 5 mmol) and NaOH (0.2 g, 5 mmol) dissolved in 10 mL of distilled water was added to an aqueous solution (25 mL) of $\text{CuSO}_4 \cdot 5\text{H}_2\text{O}$ (1.248 g, 5 mmol) with stirring for 30 min. Then 2, 2'-bipyridine (0.821 g, 5 mmol) dissolved in 10 mL of ethanol was added to the above mixture. The solution was stirred for another 2 h with heating at 333 K. After the completion of the reaction, an aqueous solution of NaClO_4 (0.700 g, 5 mmol) was added into the reaction mixture and the resultant reaction mixture was cooled down to room temperature. The mixture was filtered and the filtrate was kept for crystallization at room temperature. Block-shaped blue colour single crystals were grown from filtrate after two days which are suitable for single crystal X-ray diffraction. In the same crystallization vessel (30 mL Water:ethanol (2:1 ration v/v) mixture in 50 mL beaker), large size crystal growth was observed after 20-25 days upon slow evaporation, while standing at room temperature (30-35 °C) undisturbed. The yield of **1**: 0.64 g (78 %). Elemental composition of **1** Calc. (%): C, 44.71; H, 4.14; N, 8.23. Found (%): C, 44.62; H, 4.05; N, 8.12.

Scheme S1: Synthetic scheme followed to isolate **1**

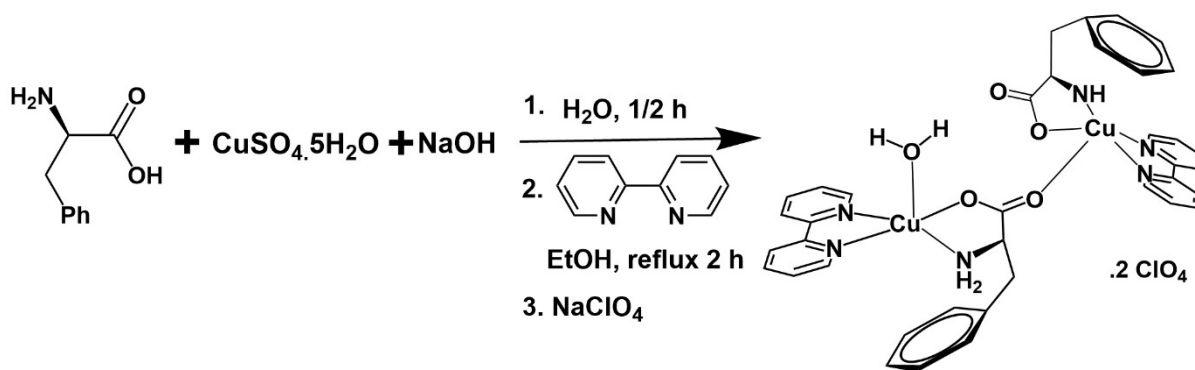


Table S1. Crystallographic parameters for complex **1**:

Parameter	1 (at 150K)	1 (at 300K)
Empirical formula	C ₃₈ H ₄₂ Cl ₂ Cu ₂ N ₆ O ₁₅	C ₃₈ H ₄₂ Cl ₂ Cu ₂ N ₆ O ₁₅
Formula weight	1020.75	1020.75
Crystal system	monoclinic	monoclinic
Space group	P2 ₁	P2 ₁
a/Å	9.3868(2)	9.4947(2)
b/Å	15.5499(3)	15.7979(3)
c/Å	14.4461(2)	14.4936(3)
β/°	93.944(2)	93.650(2)
Volume/Å ³	2103.61(7)	2169.58(8)
Z	2	2
ρ _{calc} /g/cm ³	1.612	1.563
μ/mm ⁻¹	1.215	1.179
F(000)	1048.0	1048.0
Crystal size/mm ³	0.278 × 0.25 × 0.241	0.278 × 0.25 × 0.241
Temperature/K	150.00(10)	300.00(10)
2θ _{max}	50	50
Radiation	MoK _α	MoK _α
λ [Å]	0.71073	0.71073
Reflns	43004	36696
Ind. reflns	7386	7648
Goodness-of-fit on F ²	1.029	1.032
R ₁	0.0285	0.0382
wR ₂	0.0609	0.0913

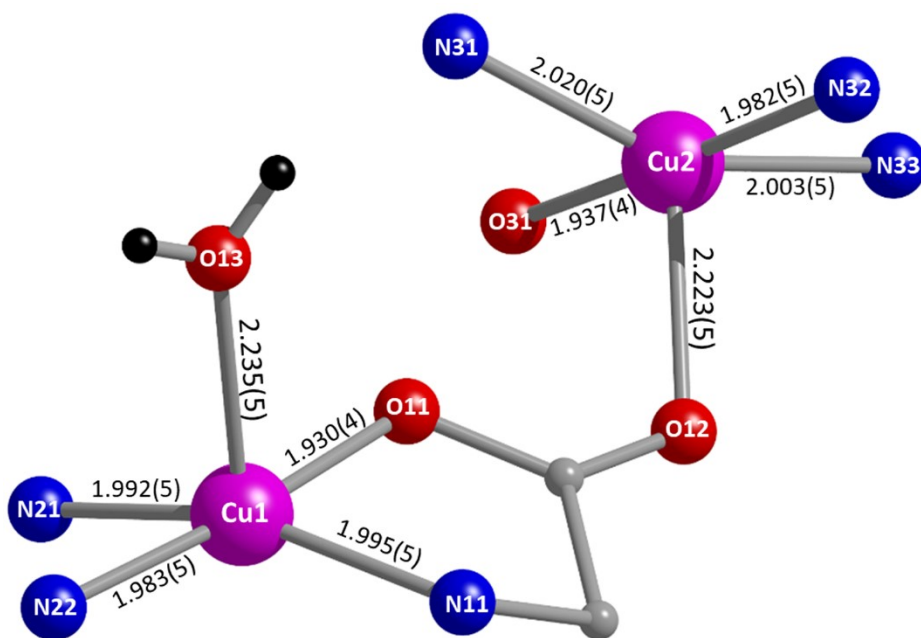


Figure S1. Selected bond lengths (in Å) of **1**.

Table S2: Selected bond angles for **1**.

Bond Angle	Value (°)	Bond Angle	Value (°)
∠N11-Cu1-N21	158.30(15)	∠N31-Cu2-N32	154.28(15)
∠N21-Cu1-N22	81.52(15)	∠N32-Cu2-N33	81.16(14)
∠N11-Cu1-O11	83.26(14)	∠N31-Cu2-O31	83.55(14)
∠N22-Cu1-O11	174.27(14)	∠N33-Cu2-O31	175.42(14)
∠O11-Cu1-O13	91.92(14)	∠O31-Cu2-O12	97.17(12)
∠N11-Cu1-O13	97.28(17)	∠N31-Cu2-O12	104.68(14)
∠N21-Cu1-O13	104.27(17)	∠N32-Cu2-O12	100.96(12)
∠N22-Cu1-O13	86.81(15)	∠N33-Cu2-O12	86.45(13)
∠N21-Cu1-O11	93.39(13)	∠N32-Cu2-O31	95.36(13)
∠N22-Cu1-N11	102.44(15)	∠N33-Cu2-N31	154.28(15)

Table S3: Atoms involved in intermolecular hydrogen bonding and its corresponding bond distances and bond angles in **1**.

H-Bond Donor(D)- Acceptor(A)	D...A (Å)	∠DHA (°)
N11-H11B...O13A_ \$1	2.995(5)	178(5)
C29-H29...O13A_ \$1	3.431(6)	120.2
N11-H11A...O2S_ \$2	2.857(5)	160(4)
O1S-H1SA...O32_ \$2	2.734(5)	137.7
C12-H12...O23A_ \$2	3.474(6)	157.6
C12-H12...O2S_ \$2	3.363(6)	103.7
O1S-H1SB...O21A_ \$3	2.974(7)	148.0
N31-H31B...O21A_ \$3	3.115(6)	162(5)
O1S-H1SB...O23A_ \$3	3.264(6)	152.1

C32-H32A...O12_\$3	3.336(5)	111.9
C45-H45...O11A_\$4	3.411(6)	162.4
C46-H46...O12A_\$4	3.493(6)	120.9
C40-H40...O14A_\$5	3.432(6)	113.1
C41-H41...O14A_\$5	3.313(6)	124.1
C37-H37...O12A_\$5	3.420(6)	125.3
C36-H36...O12A_\$5	3.448(6)	122.0
C27-H27...O24A_\$6	3.434(6)	136.3
C22-H22...O11A_\$7	3.265(6)	129.3
O2S-H2SA...O32	2.767(5)	173.1
O2S-H2SB...O22A	2.869(5)	154.0
N31-H31A...O11	2.885(5)	146(5)
O13-H13D...O14A	2.820(5)	154(7)
O13-H13C...O1S	2.658(5)	174(8)
N31-H31A...O12	3.362(5)	103(4)
N11-H11A...O13	3.179(5)	100(3)
C48-H48...N31	3.314(6)	107.3
C29-H29...N11	3.378(6)	111.6
C39-H39...O31	3.099(5)	112.5
C39-H39...O21A	3.347(6)	122.4
C20-H20...O11	3.025(6)	114.5

\$1 = -x+2, y-0.5, -z+2; \$2= x+1, y, z; \$3 = -x+1, y+0.5, -z+1; \$4 = -x+2, y-0.5, -z+1; \$5 = -x+1, y-0.5, -z+1; \$6 = -x+1, y+0.5, -z+2; \$7= x-1, y, z.

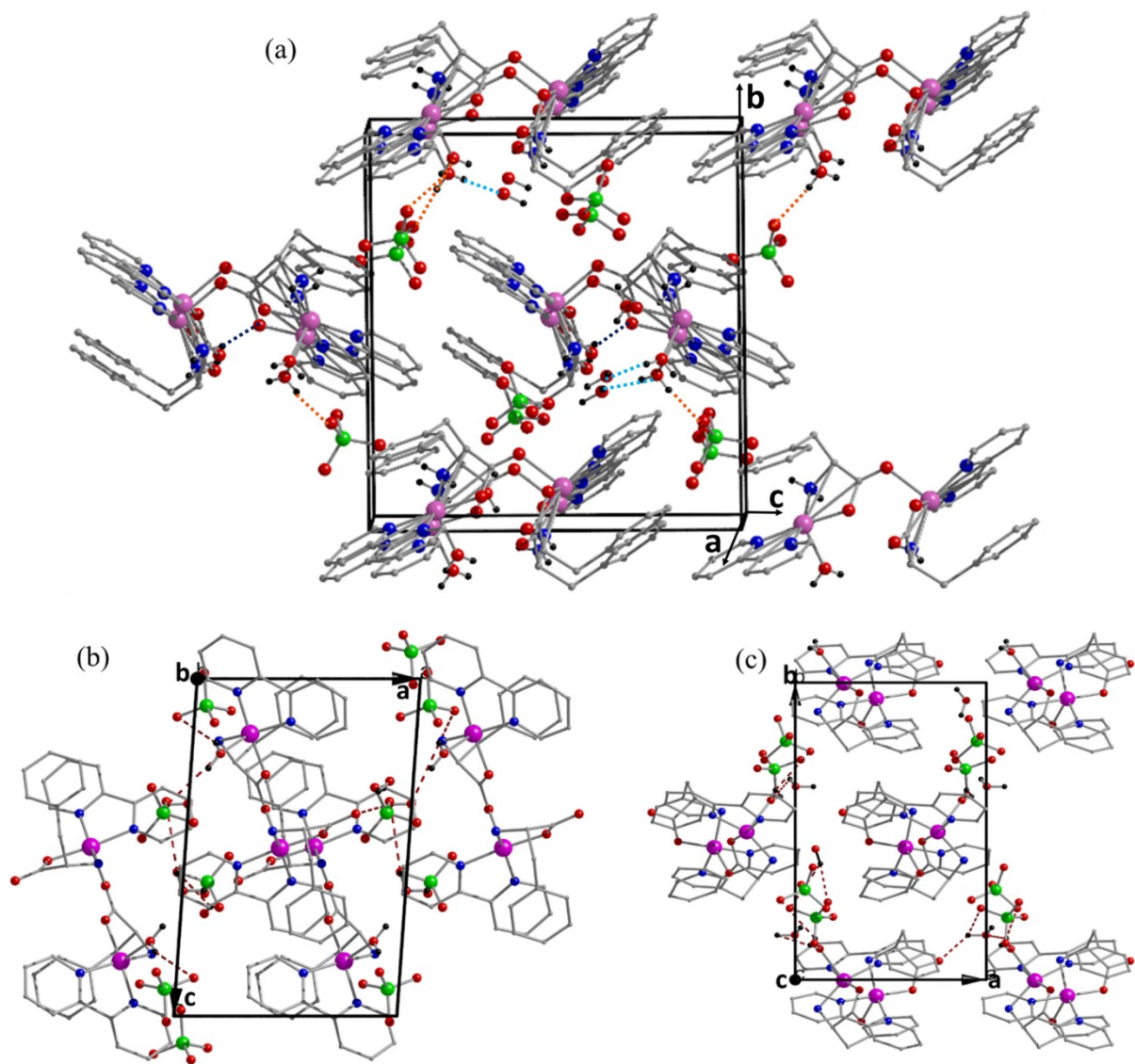


Figure S2. (a) Packing diagram of **1** along a-axis. Blue dotted lines represent O...H hydrogen bonding between the coordinated and non-coordinated water molecules, orange dotted lines represent O...H hydrogen bonding with O atom of Cl-O bond and Dark blue dotted lines represent classical H hydrogen bonding between H atoms of amine and the O atoms of the phenylalanine moiety. Colour Code: Copper: magenta; Carbon: dark grey; Nitrogen: blue; Oxygen: Red; Phosphorous: green, Fluorine: dark yellow; Hydrogen: black, (b-c) Packing diagram of **1** along b and c-axis.

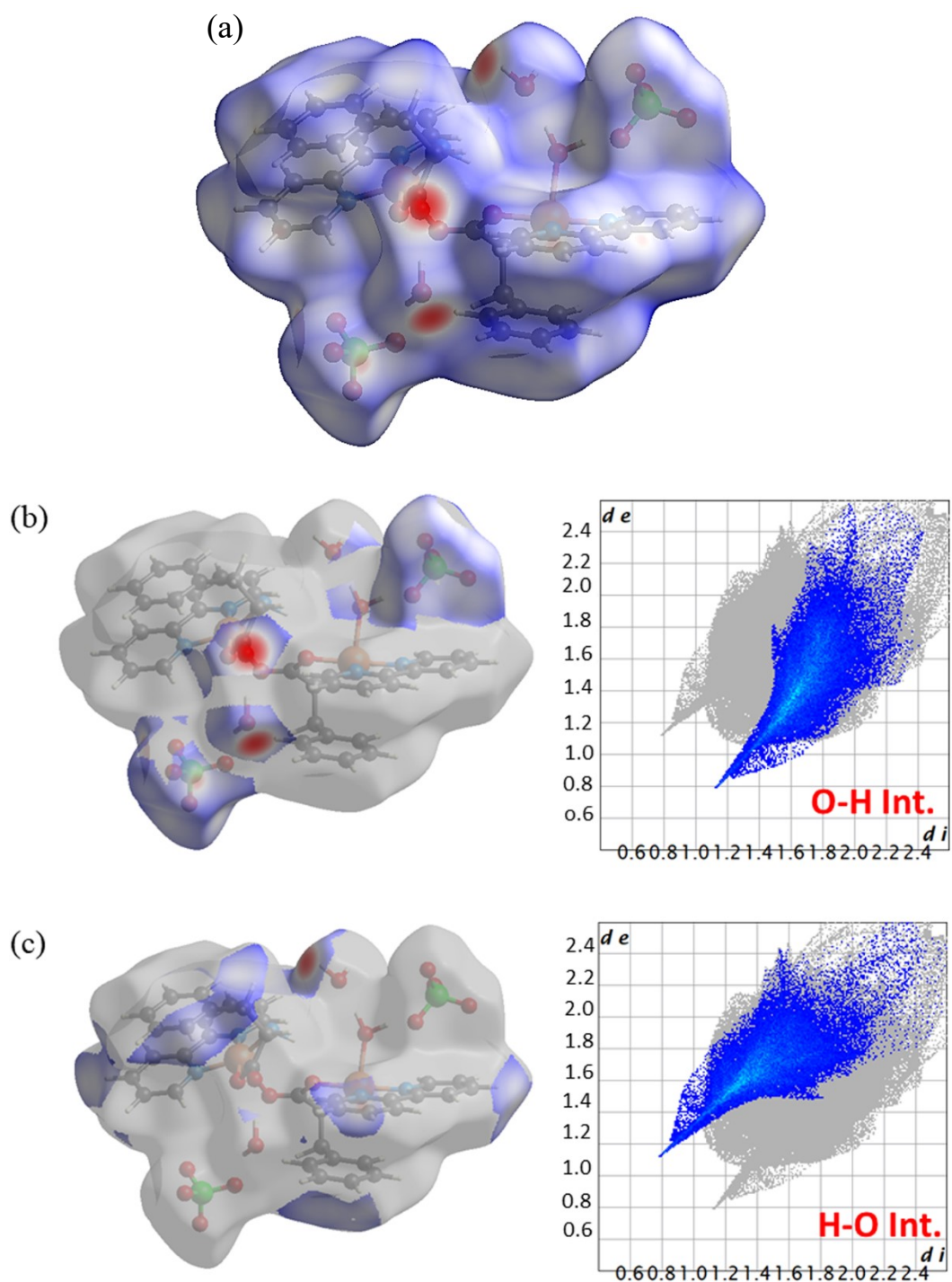


Figure S3. (a) Hirshfeld surface view of **1** and two-dimensional fingerprint plots of (b) Cl-O \cdots H (19.3%) and (c) O-H \cdots O (20.8%) interactions.

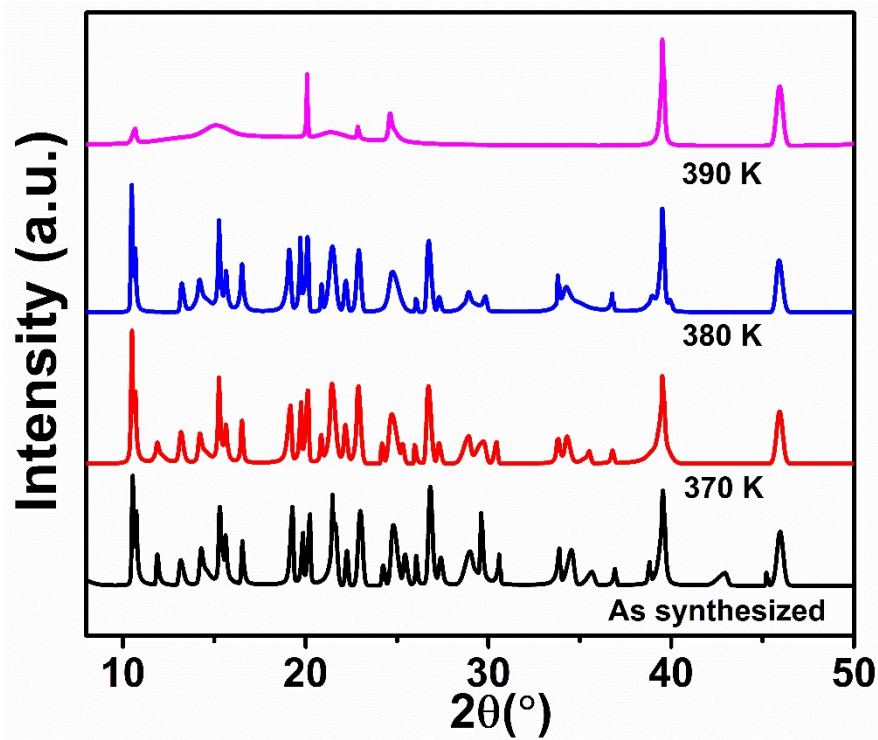


Figure S4. Variable temperature powder XRD analysis of **1**.

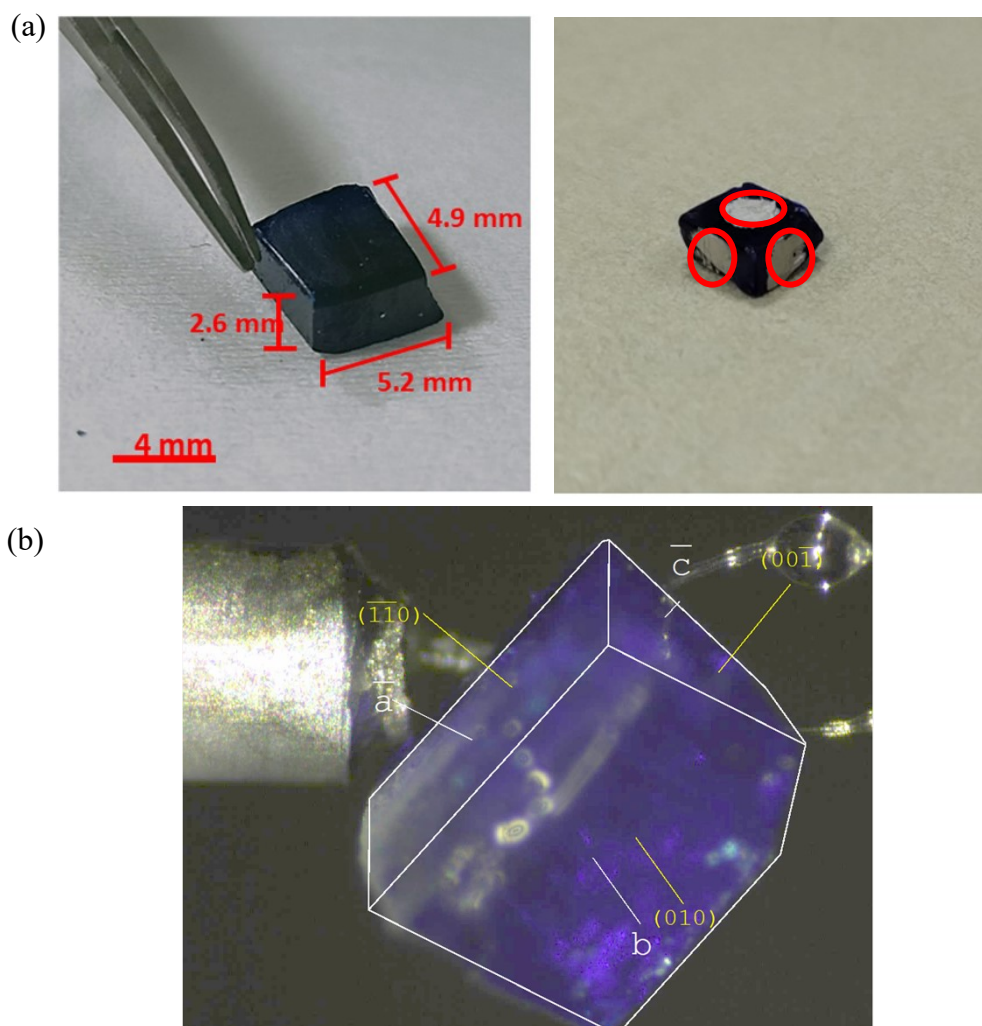


Figure S5. (a) As grown crystals (left panel) of complex **1** used for P-E loop, dielectric (right panel is showing the circular silver paste painted electrodes, used for P-E loop and dielectric study along a-, b- and c-axes) PFM measurement and piezo and pyro-electric nanogenerator (PENG) is fabrication, (b) face-indexing of the single crystal using single-crystal XRD instrument to show the planes and axes of the crystal.

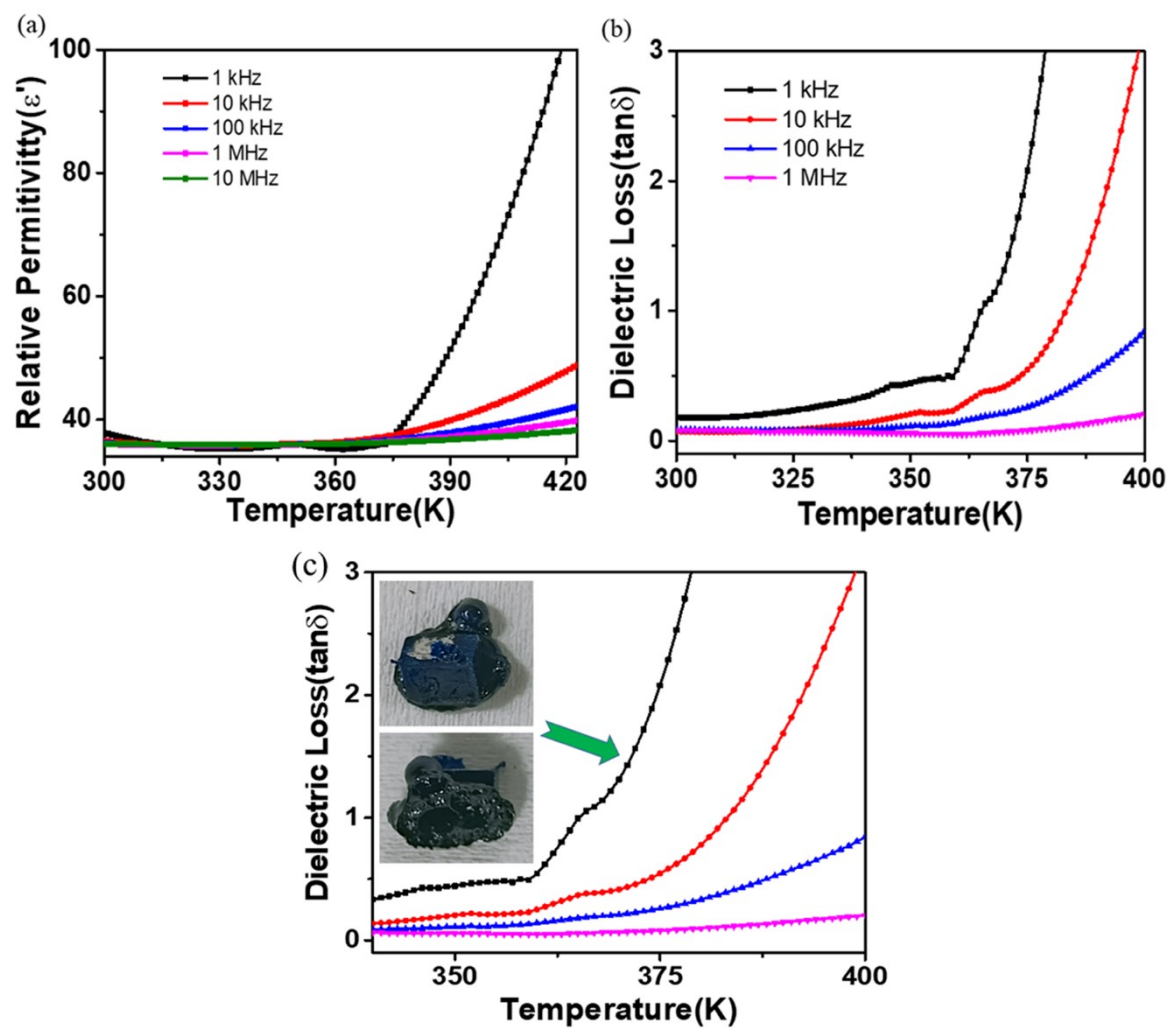


Figure S6. (a) Temperature dependence of relative dielectric permittivity (ϵ') of **1** at various frequencies, (b) Temperature dependence of dielectric loss ($\tan\delta$), (c) increase in $\tan\delta$ value due to onset of melting of the crystal.

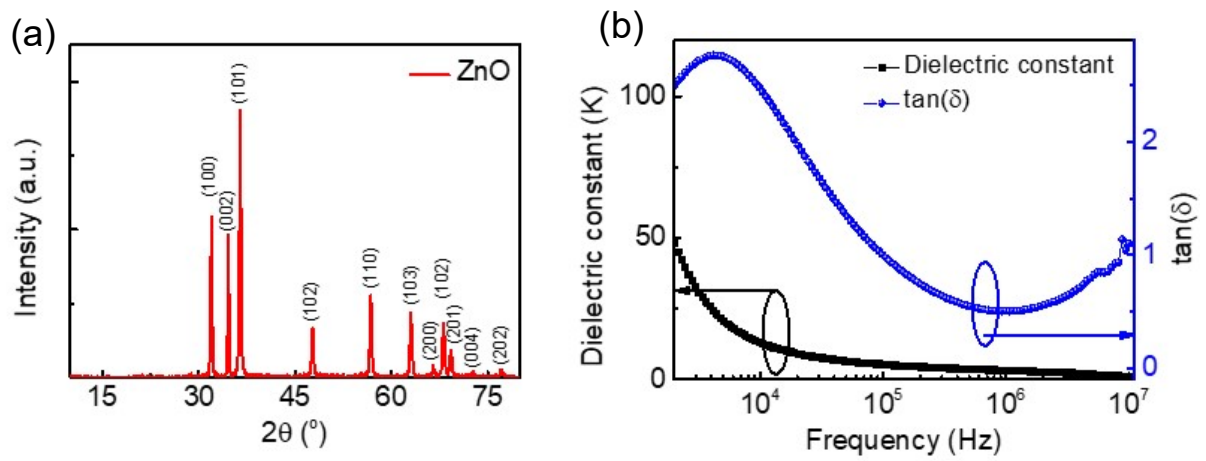


Figure S7. (a) Powder X-ray diffraction pattern of piezoelectric Wurtzite -ZnO, (b) frequency-dependent dielectric constant and loss tangent of ZnO.

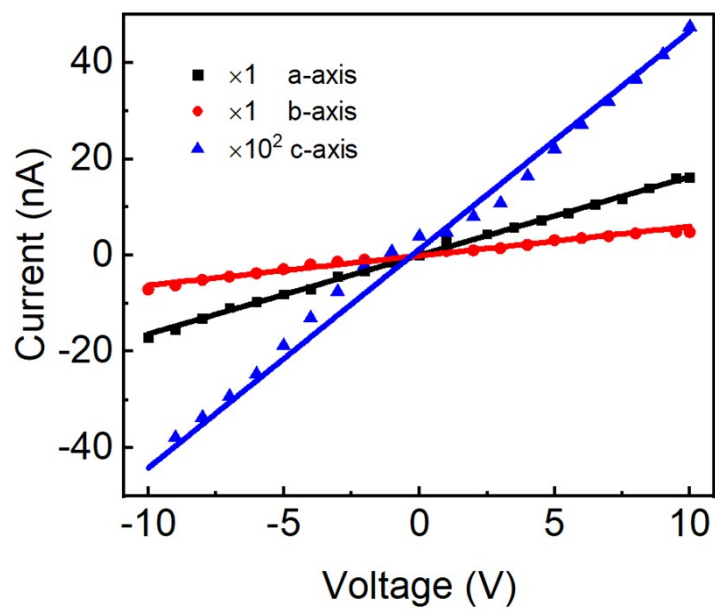


Figure S8. Current vs voltage (I-V) response of a crystal of **1** at room temperature (300 K) in a-, b- and c-axes directions describing the conducting channels in three axes attributed to charge flow due to its metallic ion centre.

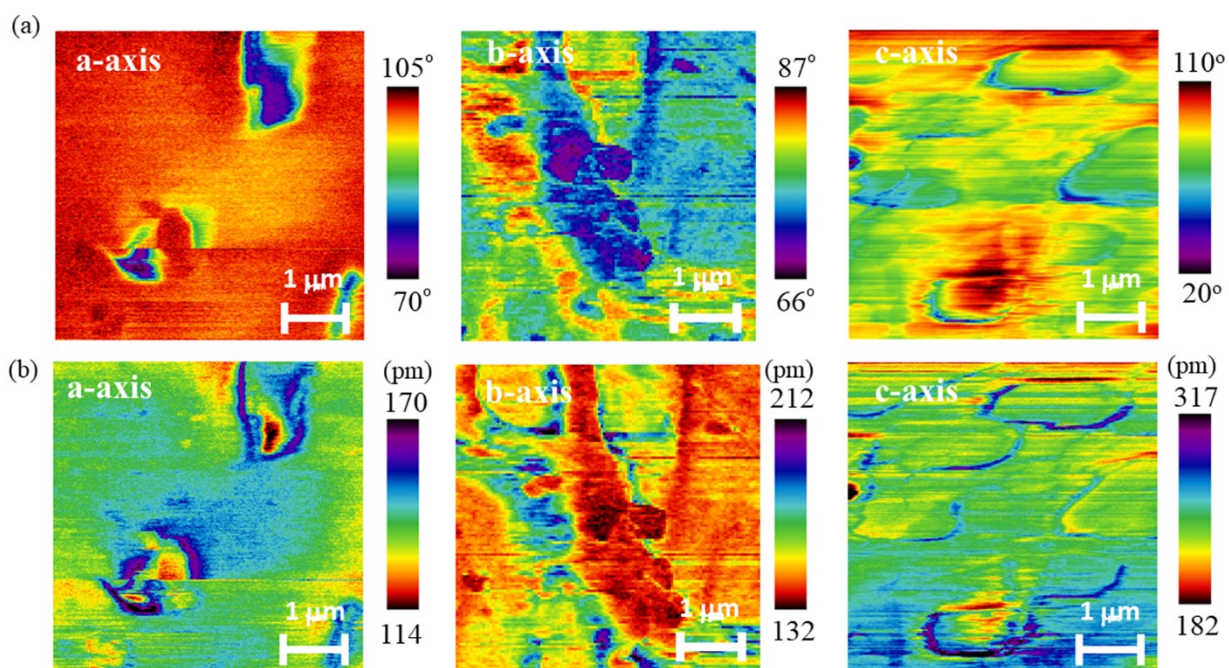


Figure S9. Lateral PFM (a) phase image of crystal **1** in a-, b- and c-axis with (b) corresponding amplitude images along these three respective axes.

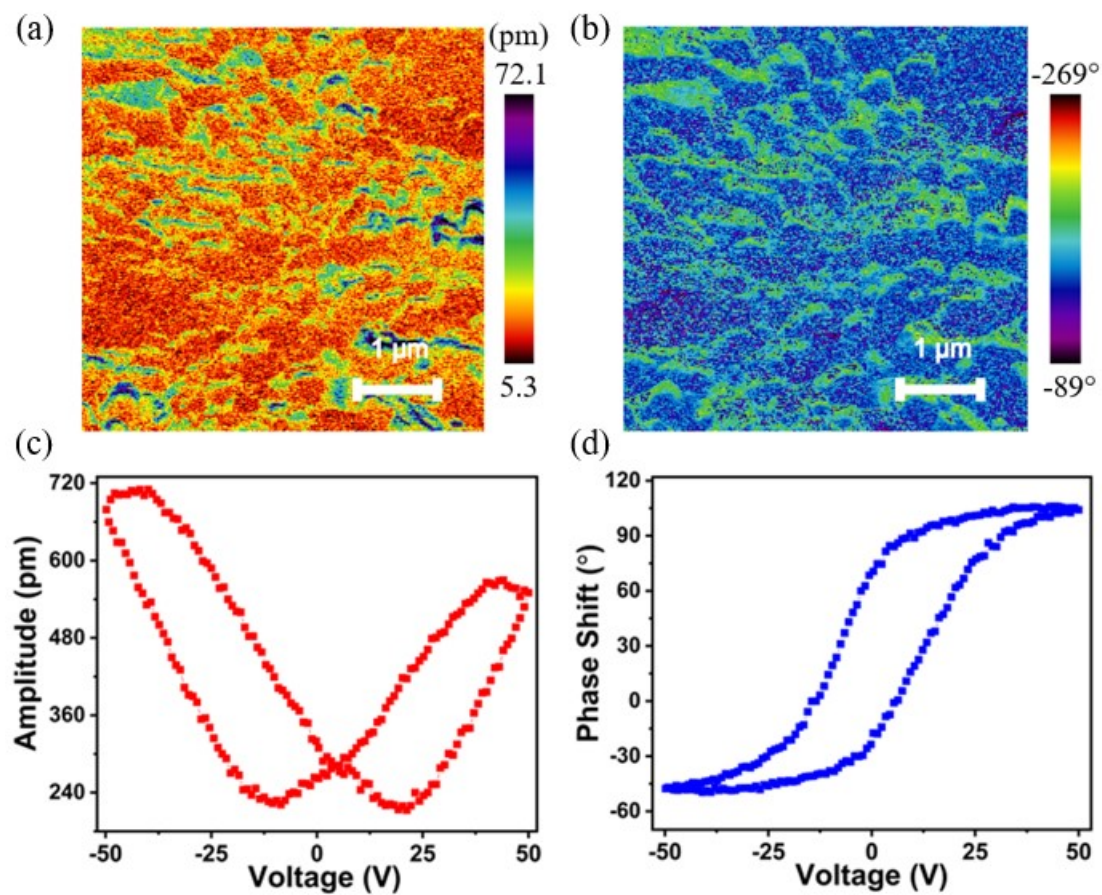


Figure S10. PFM response of a polycrystalline pellet of **1**. (a) Vertical PFM amplitude (b) corresponding phase image showing the different random domains, (c) amplitude-vs voltage butterfly loop and (d) phase shift vs voltage hysteresis loop.

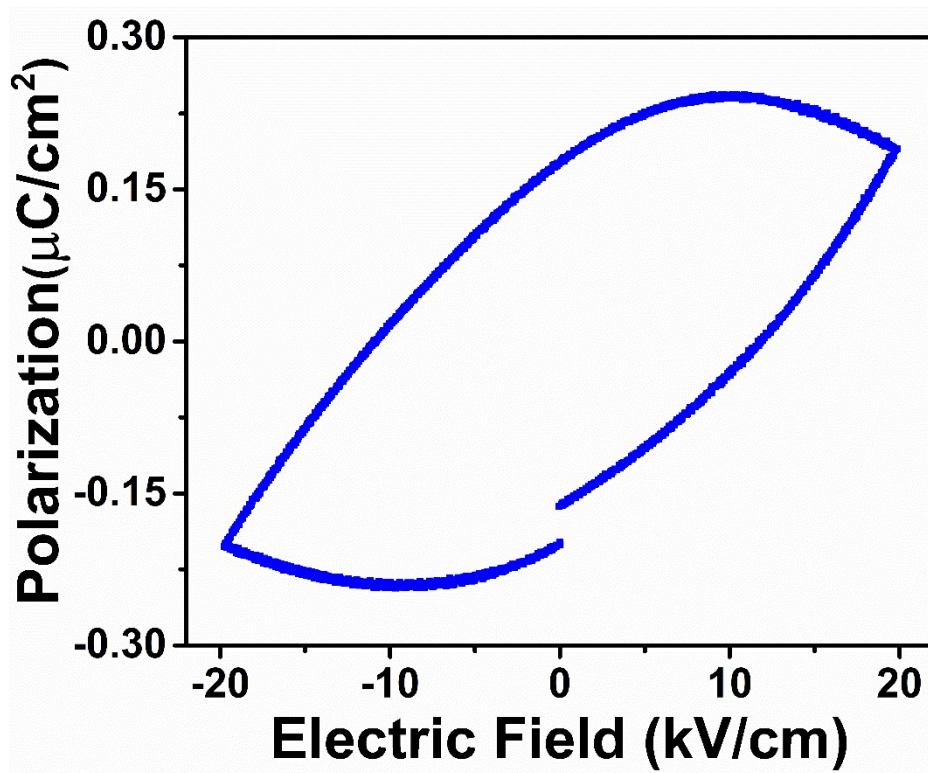


Figure S11. P-E hysteresis loop of a polycrystalline pellet of 1.

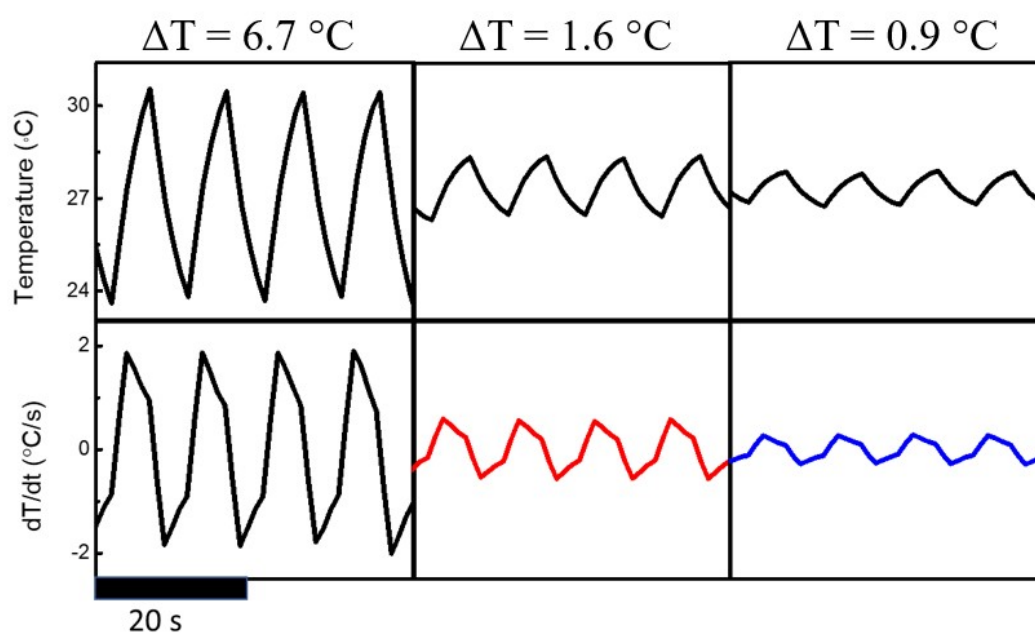


Figure S12. The input temporal heat profile (upper panel) and its first derivative (rate of change of temperature) are employed during pyroelectric current measurement which is carried out at room temperature ($\sim 300 \text{ K}$). The corresponding pyroelectric responses from PENG are shown in Figure 4 a (i~iii).